All-Printed Capacitors from Graphene-BN-Graphene Nanosheet Heterostructures

*Adam G. Kelly, David Finn, Andrew Harvey, Toby Hallam and Jonathan N. Coleman**

School of Physics, CRANN and AMBER Research Centers, Trinity College Dublin, Dublin 2, Ireland

*colemaj@tcd.ie

Abstract

This work aims to develop methodologies to print pinhole-free, vertically-stacked heterostructures by sequential deposition of conductive graphene and dielectric *h*-BN nanosheet networks. We achieve this using a combination of inkjet printing and spray-coating to fabricate dielectric capacitors in a stacked graphene/BN/graphene arrangement. Impedance spectroscopy shows such heterostructures to act as series combinations of a capacitor and a resistor, with the expected dimensional dependence of the capacitance. The areal capacitance ranges from 0.24 to 1.1 nF/cm^2 with an average series resistance of ~120 kΩ. The sprayed BN dielectrics are pinhole-free for thicknesses above 1.65 μm. This development paves the way toward fabrication of all-printed, vertically integrated, multilayer devices.

For fifty years, advances in electronics have been associated with the ever-increasing drive to produce smaller, faster silicon-based transistors. However, more recently the drive toward applications in wearable electronics, passive RFIDs and the Internet of Things has created a demand for cheap, flexible, disposable electronic devices and circuitry.[1-3] As a result, the field of printed electronics (PE) has exploded to meet this demand. PE generally involves using deposition processes associated with printing, such as such inkjet printing and spray-coating, to fabricate all aspects of devices.[4,5] Further development of this area will require using new nano-materials to produce advanced inks with superior properties, but which can deposited using existing printing methods.

Until very recently, printed electronics has been dominated by inks loaded with organics or conjugated polymers in both metallic and semiconducting form which have been used to print active layers or highly conductive traces.[6] A range of devices, including LEDs, thin-film transistors and solar cells, fabricated using printing techniques, have demonstrated impressive performance.[7-9] However, organic materials have mobilities which are limited to a few cm^2/Vs.[10] This has led some researchers to propose inks based on inorganic particles which have inherently higher mobility than organics. We, and others, have suggested that the family of 2-dimensional nanomaterials is an attractive candidate for use in PE.[11,12]

Over the last few years, it has been comprehensively shown that liquid dispersions of 2D nanosheets can be produced in large quantities by liquid phase exfoliation.[13,14] A host of 2D materials including graphene, BN, MoS_2 and GaS have been dispersed as mono- to few-layer nanosheets in solvents suitable for printing.[15-17] Such dispersions (referred to as inks when their properties are tailored for a deposition process) show excellent compatibility with solution-based deposition. The refinement of a dispersion into an ink requires certain criteria to be met. For

inkjetting, rheological parameters must lie within a specified range of the inverse Ohnesorge number,[18] $Z = \sqrt{\gamma\rho a} / \eta$ (γ, ρ and η are the ink surface tension, density and viscosity while a is the nozzle diameter (21 μm in our case)) which is typically in the range $1 \leq Z \leq 14$, although this is not a stringent condition.[19] In addition a balance of concentration and flake size is necessary to prevent nozzle clogging.[18,20] Spray-coating, on the other hand, has a much higher parameter tolerance since a larger nozzle size allows larger flakes to be deposited and atomisation at the airbrush tip means viscosity and surface energy of the solvent play a much smaller role.[21]

Inks composed of graphene[11,20,22,23] and MoS_2[20,24] nanosheets have shown excellent potential for electronics applications. However, due to the nascent nature of the field, work has predominantly focused on investigating the efficacy of established deposition methods and ink development. To date, all-printed devices have been relatively simple and have generally been planar in structure.[20,24] Limitations of the printing method become apparent when one considers the nature of the deposited films themselves. A printed film composed purely of 2D materials is a porous nanoflake network (PNN). Such systems are prone to non-uniformities, which may act as pinholes, resulting in undesired contact between layers.[25] This is a critical limitation as it will prevent the construction of heterostacks and therefore many device geometries. The development of a protocol for creating pinhole-free films is thus essential for the advancement of printed electronics. We believe the best way to approach this is to study the printing of capacitors from vertically stacked films of nanosheets. Such a heterostack will function as a capacitor only when the dielectric layer is pinhole free.

Printed capacitors have traditionally employed a polymer as a dielectric layer,[26,27] careful selection of which has allowed features such as transparency to be incorporated.[28] While capacitors have been created using CVD-grown 2D *h*BN,[29] this method is currently incompatible with printed

electronics. Recently, a nanosheet dielectric was demonstrated with montmorillonite clay acting as a high performance dielectric.[30] In the current study, a process has been developed which incorporates inkjet printing of conductive graphene electrodes and spray-coating of a pinhole-free dielectric boron nitride layer with thicknesses ranging from 1.65 to 5.15 μm. The devices displayed capacitances ranging from 0.24 to 1.1 nF/cm^2, indicating the creation of pinhole-free films.

In order to fabricate a fully solution-processed 2D material device, we employed well-established liquid-phase exfoliation techniques to produce our inks.[14-16] While inks based on semi-metal[18,20] and semiconducting[12,24] 2D nanosheets have already been demonstrated, no devices have been constructed with insulating/dielectric regions fabricated from BN nanosheet-based inks. To remedy this, we have developed a BN ink based on our graphene ink production protocol.[20] In particular, the size of the graphene flakes was chosen to be $<a/50$ *i.e.* <420 nm to avoid nozzle clogging. Briefly, graphene and BN layered powders were exfoliated by tip-sonication in NMP and isopropanol respectively (50 mg/ml) at 120 W for 7 hrs. A two-step liquid cascade centrifugation[31] (graphene; centrifuged at 546g for 90 min, collection of supernatant followed by centrifugation at 1257g for 90 min and redispersion of sediment. BN; same procedure but centrifugation speeds were 120g and 426g) was applied to concentrate and size select the nanosheets resulting in inks of concentration 1.6 mg/ml (graphene) and 0.5 mg/ml (BN). TEM images of representative flakes are shown in Figures 1(a) and 1(b). Statistical analysis showed the nanosheet lateral dimensions to be $<L>$ ~195 nm for graphene and ~450 nm for boron nitride. Shown in Figure 1(c) is an extinction spectrum measured for a graphene ink. Using published

metrics,[32] we can use the ratio of the extinction at the long-wavelength plateau to that at the peak to deduce the mean nanosheet thickness to be ~8 monolayers.

As the graphene was dispersed in NMP (Z=17, close enough to the prescribed range), no additions to the solvent vehicle were necessary to tune the rheology.[18,20] The BN ink was produced using isopropanol as the stabilising solvent due to its low boiling point, non-toxicity and reasonable surface energy matching with boron nitride.[13] The change of solvent here also serves a second function; when depositing the second layer of a heterostack with an ink using the same solvent as the first layer, the interface between the films is prone to redispersion on contact with the solvent. This is particularly true for high boiling point solvents such as NMP where films retain residual solvent even after an annealing step.[14] We note that inks for spray coating do not require the detailed tuning of dispersion properties that is necessary for inkjet printing, thus allowing a larger lateral flake size for the BN ink.

Using these differing solvent vehicles, the inks can easily be printed (graphene) and sprayed (BN) to give individual lines or films. SEM inspection of such single-layer films (inkjet-printed graphene in Figure 1(d) and spray-coated boron nitride in Figure 1(e)) shows excellent film continuity across large distances and further magnification shows our films to be PNNs with considerable porosity.

While many papers have reported printing films and lines of 2D nanosheets, much less work has focused on printing device structures. The capacitors produced here consist of stacked heterostructures of graphene/boron-nitride/graphene nanosheet networks (Figures 1(f-h)), combining inkjet printing and spray-coating techniques. The bottom (and top) electrodes (roughly 4 mm × 1 mm) were deposited using a drop-on-demand inkjet printer (Dimatix DMP 2800) onto an alumina-coated PET substrate specially designed to minimise droplet wetting. In line with our

previous work, the graphene electrodes are fabricated using 20 passes of the printer, yielding a thickness of ~400 nm.[20] The BN dielectric layer was spray-coated on top of the bottom graphene electrode using a Harder & Steenbeck Infinity Airbrush secured to a Janome JR2300N mobile gantry. The spray-coating method allows deposition of large volumes of material in homogeneous, large area films. Preliminary experiments showed this method gave pinhole-free dielectric layers albeit at thickness >1.65 μm. The top electrode was then deposited by inkjet printing in a manner identical to the bottom electrode to give an electrode overlap area of ~1 mm^2. Raman analysis (Figure 1(i)) shows the different device regions to give the expected spectra[33,34] demonstrating the fidelity of materials deposition. Finally, the edges of the electrode were coated with silver paste contact pads to facilitate connection to the needle probes.

In order to characterise the properties of the capacitors, impedance spectra (measured with a Gamry 3000) were recorded for a range of capacitors with varying thickness and overlap area. Figures 2(a) and 2(b) show representative Bode plots for a capacitor with dielectric thickness of 4.15 μm and a 2.5 mm^2 electrode overlap area. These data are typical of a series *R*-*C* equivalent circuit; a dominating resistive component *R* (Z_{Real}) with a corresponding phase angle approaching 0° at high frequencies while at low frequencies the fully capacitive interface dominates the impedance as the phase shift approaches -90°. For a series *R*-*C* combination (figure 2(a) inset), the impedance can be represented as

$$Z = Z_{\mathrm{Re}} + iZ_{\mathrm{Im}} = R_{Ser} - i/\omega C \qquad (1)$$

where R_{SER} is the series resistance and *C* is the capacitance. Under these circumstances, impedance amplitude and phase angle are given by

$$|Z| = \sqrt{R_{Ser}^2 + (\omega C)^{-2}} \qquad (2)$$

and

$$\phi = \tan^{-1}(1/\omega R_{Ser} C) \quad (3)$$

Fitting these equations to the data gives good agreement and, for the device plots shown in Figures 2(a) and 2(b), gives a series resistance of 125 kΩ, a capacitance of 6.13 pF (0.245 nF/cm^2) and an *RC* time constant of 0.74 μs in this geometry. We note that this series resistance is significantly greater than the ~2 kΩ which would be expected from the electrodes given the in-plane conductivity of liquid exfoliated graphene films of ~10^4 S/m.[35] We attribute this to the significant out-of-plane nature of the current flow in these capacitors. By comparison with measurements on MoS_2 nanosheet networks,[36,37] we would expect the out-of-plane conductivity of graphene networks to be up to ×1000 lower than the in-plane value, contributing greatly to the series resistance.

We can use the impedance data to directly calculate the frequency dependence of the relative permittivity, ε_r. To this we first calculate the complex capacitance using $C(\omega) = [i\omega Z(\omega)]^{-1}$. We then transform the real part of the capacitance into the frequency dependent relative permittivity using the standard expression:

$$C = \varepsilon_r \varepsilon_0 A / t \quad (4)$$

where *t* is the thickness of the BN dielectric film, *A* is the electrode overlap area and the other symbols have their usual meaning. We have plotted $\varepsilon_r(\omega)$ versus ω in Figure 2(c) for capacitors with three different BN film thicknesses. For $\omega < 3\times10^5$ rad/s, the relative permittivity was invariant with both thickness and frequency at ~2-2.5, in agreement with previous reports.[38] For higher frequencies, $\varepsilon_r(\omega)$ fell off as expected for a standard dielectric.

An array of such capacitors was then fabricated to confirm the scaling of capacitance with dimensions as given by equation 4. This was done by inkjet printing a uniform 4×4 arrangement

of graphene bottom electrodes, indicated in Figure 1(e), upon which a polymer mask was placed and the boron nitride ink was spray-coated over. Thickness variation of the boron nitride layer was achieved by closing off successive holes in the mask after 30 ml of ink had been sprayed. The top electrodes were then inkjet printed onto the dielectric layer with the overlap area varied by modulating the electrode width, Δx, as shown in Figure 1(e). The capacitance was extracted by fitting the impedance data using equations 2 and 3.

Figures 3(a) – 3(c) show the behavior expected for pinhole-free dielectric layers. Figure 3(a) shows data holding the area constant at A=1 mm^2, while thickness was varied from t=1.65 μm to 5.15 μm and is consistent with $C \propto 1/t$. The lower limit at which spray-deposition produced short-free BN films was found to be 1.65 μm. However, we are confident that thinner, yet pinhole-free, films should be achievable through further tailoring of dispersion properties and deposition parameters. Figure 3(b) shows capacitance data from devices where thickness was held constant at t=4.15 μm while the area is varied from A=0.5 to 2.5 mm^2 and here we see the expected linear relationship in excellent agreement with Equation 4. Figure 3(c) shows the capacitance of all devices plotted against their ratio of area to thickness, again showing good consistency with Equation 4. From the slope we extract an average dielectric constant, ε_r, of ~1.63, in reasonable agreement with the low frequency data shown in Figure 2(c). We note that this value refers to the porous network and, assuming a porosity of 50%, implies a BN dielectric constant of 2.25, which is consistent with the value of 3±1 reported for the out-of-plane permittivity of layered BN.[38] We have also calculated the relative permittivity for each capacitor separately which we plot versus A/t in Figure 3(d). We see relatively low scatter suggesting our fabrication method to be relatively reproducible.

In conclusion, we have created a graphene/boron nitride capacitive heterostructure using a combination of inkjet printing and spray-coating deposition techniques. The viability of these devices means that pinhole-free BN networks were achieved. These devices show areal capacitance ranging from 0.24 to 1.1 nF/cm^2 with a limiting dielectric thickness of 1.65 μm. We believe this work is an important step in the growing field of printed electronics, in particular the realisation of all-printed heterostructures from solution-processed 2D materials.

While these early results are promising, future work will involve refining the printing process to give thinner dielectric films that remain pinhole-free. Furthermore, the dielectric layer should also be inkjet printed to consolidate the entire deposition process and this should be achievable through further refinement of the boron nitride dispersions.

Funding Sources

This work was primarily supported by the SFI-funded AMBER research centre (SFI/12/RC/2278) as part of the platform projects program. In addition, we acknowledge Science Foundation Ireland (11/PI/1087) and the European Research Council (SEMANTICS) for continuing support. We have also received funding from the European Union Seventh Framework Program under grant agreement n°604391 Graphene Flagship.

Figures

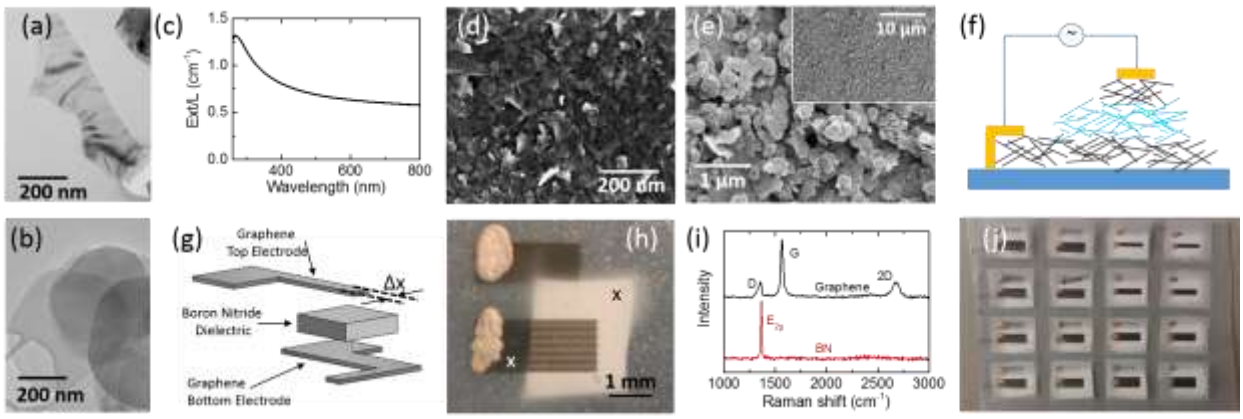

Figure 1: Material/Device Overview. (a-b) Representative TEM images of graphene (a) and BN (b) nanosheets. (c) Extinction spectrum (expressed as extinction per cell length) of a graphene dispersion. (d-e) SEM image of printed graphene (d) and sprayed BN (e) networks. (e, inset) Lower magnification image showing a pinhole-free BN film. (f-g) Vertically stacked graphene/boron nitride/graphene heterostructures shown both conceptually (f) and schematically (g). (h) Photograph of a printed capacitor. The white structure is BN while the black rectangles are graphene. The gray blobs are silver paint contact pads. The horizontal features on the top graphene electrode are swath lines, a common source of non-uniformity often found in ink-jet printing.[20] The black and white x symbols mark the approximate positions where Raman spectra were collected. (i) Raman spectra collected from the graphene and BN portions of a capacitor. (j) Photograph of a sample array of working devices; columns 1 and 2 have area held constant while thickness varies while columns 3 and 4 have thickness held constant while area varies.

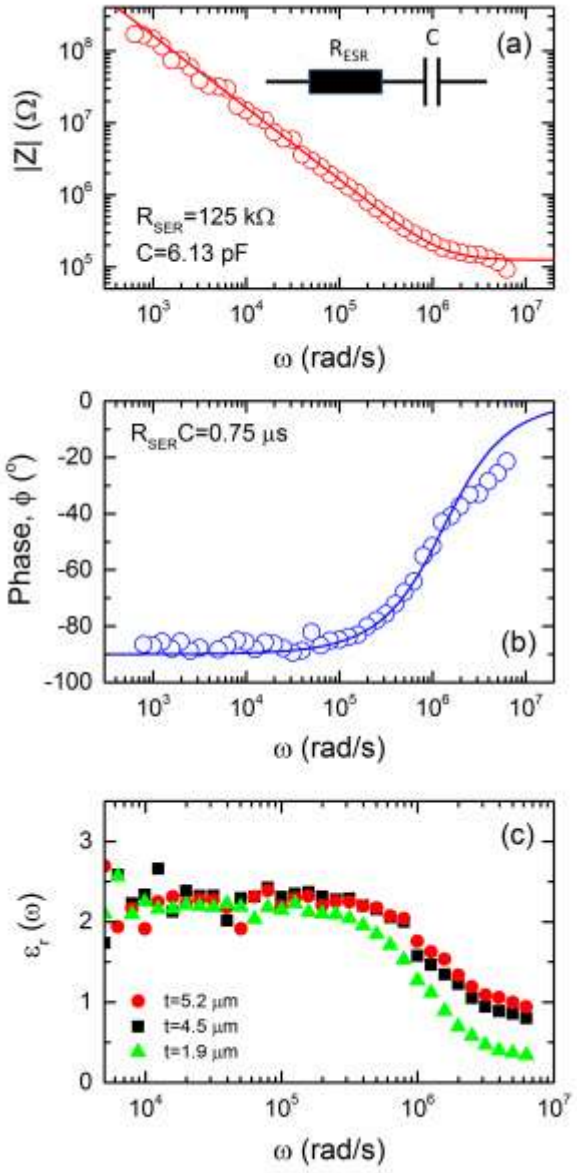

Figure 2: (a-b) Representative Bode plots for a typical capacitor. (a) Impedance amplitude, $|Z|$, and (b) phase angle, ϕ, as a function of angular frequency, ω. The lines represent fits to an equivalent series *R*-*C* series circuit, shown in inset in (a). Fit constants are given in the panels. (c) Frequency dependence of the relative permittivity (calculated from the real part of the capacitance using $C(\omega) = \left[i\omega Z(\omega)\right]^{-1}$) for three different BN film thicknesses.

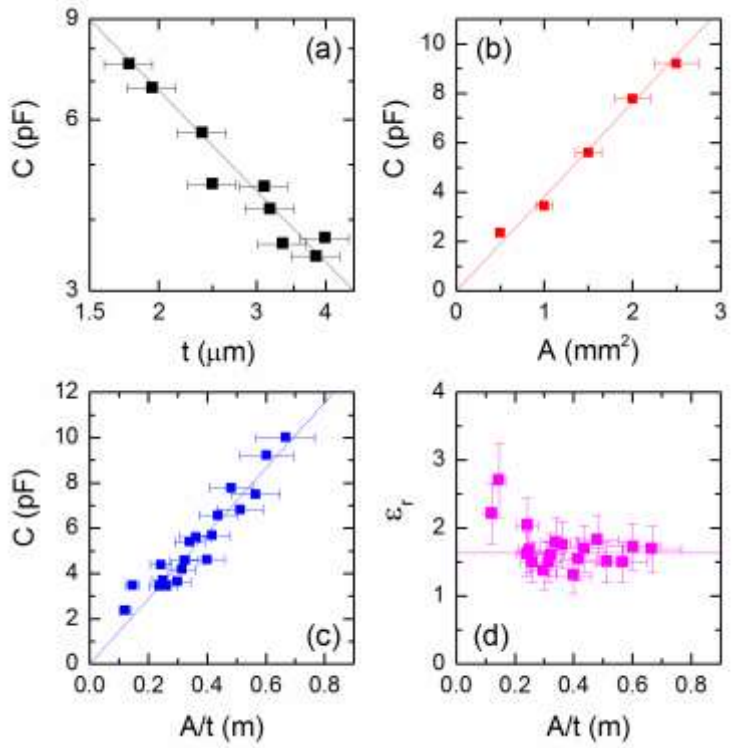

Figure 3: Capacitance values extracted from impedance fits for all data sets. (a) Absolute capacitance plotted as a function of the boron nitride thickness, *t*, with area held constant at *A*=1 mm^2. (b) Absolute capacitance plotted as a function of area, A, with thickness held constant at t=4.15 μm. (c) Absolute capacitance plotted as a function of the ratio of area to thickness, *A/t*. (d) Relative permittivity of individual capacitors plotted versus *A/t*.

References

1 G. A. Casula, G. Montisci, and G. Mazzarella, Ieee Antenn Wirel Pr **12**, 1400 (2013).

2 Y. Li, R. Torah, S. Beeby, and J. Tudor, 2012 Symposium on Design, Test, Integration and Packaging of Mems/Moems (Dtip), 192 (2012).

3 D. O. Oyeka, M. A. Ziai, J. C. Batchelor, E. A. Parker, V. Sanchez-Romaguera, and S. G. Yeates, Ieee Antennas Prop, 1726 (2013).

4 F. C. Krebs, Sol Energ Mat Sol C **93** (4), 394 (2009).

5 H. F. Castro, E. Sowade, J. G. Rocha, P. Alpuim, S. Lanceros-Méndez, and R. R. Baumann, Journal of Elec Materi **43** (7), 2631 (2014).

[6] Y. Aleeva and B. Pignataro, J. Mater. Chem. C **2** (32), 6436 (2014).
[7] S. Kola, J. Sinha, and H. E. Katz, J Polym Sci Pol Phys **50** (15), 1090 (2012).
[8] T. Kawase, T. Shimoda, C. Newsome, H. Sirringhaus, and R. H. Friend, Thin Solid Films **438**, 279 (2003).
[9] N. C. van der Vaart, H. Lifka, F. P. M. Budzelaar, J. E. J. M. Rubingh, J. J. L. Hoppenbrouwers, J. F. Dijksman, R. G. F. A. Verbeek, R. van Woudenberg, F. J. Vossen, M. G. H. Hiddink, J. J. W. M. Rosink, T. N. M. Bernards, A. Giraldo, N. D. Young, D. A. Fish, M. J. Childs, W. A. Steer, D. Lee, and D. S. George, J Soc Inf Display **13** (1), 9 (2005).
[10] Hagen Klauk, Marcus Halik, Ute Zschieschang, Günter Schmid, Wolfgang Radlik, and Werner Weber, Journal of Applied Physics **92** (9), 5259 (2002).
[11] F. Torrisi and J. N. Coleman, Nat Nanotechnol **9** (10), 738 (2014).
[12] F. Withers, H. Yang, L. Britnell, A. P. Rooney, E. Lewis, A. Felten, C. R. Woods, V. S. Romaguera, T. Georgiou, A. Eckmann, Y. J. Kim, S. G. Yeates, S. J. Haigh, A. K. Geim, K. S. Novoselov, and C. Casiraghi, Nano Lett **14** (7), 3987 (2014).
[13] Jonathan N. Coleman, Mustafa Lotya, Arlene O'Neill, Shane D. Bergin, Paul J. King, Umar Khan, Karen Young, Alexandre Gaucher, Sukanta De, Ronan J. Smith, Igor V. Shvets, Sunil K. Arora, George Stanton, Hye-Young Kim, Kangho Lee, Gyu Tae Kim, Georg S. Duesberg, Toby Hallam, John J. Boland, Jing Jing Wang, John F. Donegan, Jaime C. Grunlan, Gregory Moriarty, Aleksey Shmeliov, Rebecca J. Nicholls, James M. Perkins, Eleanor M. Grieveson, Koenraad Theuwissen, David W. McComb, Peter D. Nellist, and Valeria Nicolosi, Science **331** (6017), 568 (2011).
[14] Y. Hernandez, V. Nicolosi, M. Lotya, F. M. Blighe, Z. Y. Sun, S. De, I. T. McGovern, B. Holland, M. Byrne, Y. K. Gun'ko, J. J. Boland, P. Niraj, G. Duesberg, S. Krishnamurthy, R. Goodhue, J. Hutchison, V. Scardaci, A. C. Ferrari, and J. N. Coleman, Nat Nanotechnol **3** (9), 563 (2008).
[15] J. N. Coleman, M. Lotya, A. O'Neill, S. D. Bergin, P. J. King, U. Khan, K. Young, A. Gaucher, S. De, R. J. Smith, I. V. Shvets, S. K. Arora, G. Stanton, H. Y. Kim, K. Lee, G. T. Kim, G. S. Duesberg, T. Hallam, J. J. Boland, J. J. Wang, J. F. Donegan, J. C. Grunlan, G. Moriarty, A. Shmeliov, R. J. Nicholls, J. M. Perkins, E. M. Grieveson, K. Theuwissen, D. W. McComb, P. D. Nellist, and V. Nicolosi, Science **331** (6017), 568 (2011).
[16] U. Khan, A. O'Neill, M. Lotya, S. De, and J. N. Coleman, Small **6** (7), 864 (2010).
[17] Graeme Cunningham, Mustafa Lotya, Clotilde S. Cucinotta, Stefano Sanvito, Shane D. Bergin, Robert Menzel, Milo S. P. Shaffer, and Jonathan N. Coleman, Acs Nano **6** (4), 3468 (2012).
[18] Felice Torrisi, Tawfique Hasan, Weiping Wu, Zhipei Sun, Antonio Lombardo, Tero S. Kulmala, Gen-Wen Hsieh, Sungjune Jung, Francesco Bonaccorso, Philip J. Paul, Daping Chu, and Andrea C. Ferrari, Acs Nano **6** (4), 2992 (2012).
[19] P. Shin, J. Sung, and M. H. Lee, Microelectron Reliab **51** (4), 797 (2011).
[20] David J. Finn, Mustafa Lotya, Graeme Cunningham, Ronan J. Smith, David McCloskey, John F. Donegan, and Jonathan N. Coleman, J. Mater. Chem. C **2** (5), 925 (2014).
[21] V. Scardaci, R. Coull, and J. N. Coleman, Appl Phys Lett **97** (2) (2010).
[22] E. B. Secor, S. Lim, H. Zhang, C. D. Frisbie, L. F. Francis, and M. C. Hersam, Adv Mater **26** (26), 4533 (2014).
[23] F. Torrisi, T. Hasan, W. P. Wu, Z. P. Sun, A. Lombardo, T. S. Kulmala, G. W. Hsieh, S. J. Jung, F. Bonaccorso, P. J. Paul, D. P. Chu, and A. C. Ferrari, Acs Nano **6** (4), 2992 (2012).

[24] Chuanbao Cao Youqi Zhu, Shi Tao, Wangsheng Chu, Ziyu and Yadong Li, Scientific Reports **5787** (4) (2014).
[25] Z. C. Ding, R. B. Xing, Q. A. Fu, D. G. Ma, and Y. C. Han, Org Electron **12** (4), 703 (2011).
[26] B. S. Cook, J. R. Cooper, and M. M. Tentzeris, Ieee Microw Wirel Co **23** (7), 353 (2013).
[27] Yi Li, R. Torah, S. Beeby, and J. Tudor, presented at the 2012 IEEE Sensors, 2012 (unpublished).
[28] S. Sorel, U. Khan, and J. N. Coleman, Appl Phys Lett **101** (10), 103106 (2012).
[29] Ning Guo, Jinquan Wei, Yi Jia, Huanhuan Sun, Yuhang Wang, Kehan Zhao, Xiaolan Shi, Liuwan Zhang, Xinming Li, Anyuan Cao, Hongwei Zhu, Kunlin Wang, and Dehai Wu, Nano Res **6** (8), 602 (2013).
[30] J. Zhu, X. L. Liu, M. L. Geier, J. J. McMorrow, D. Jariwala, M. E. Beck, W. Huang, T. J. Marks, and M. C. Hersam, Adv Mater **28** (1), 63 (2016).
[31] Claudia Backes, Beata M. Szydlowska, Andrew Harvey, Shengjun Yuan, Victor Vega-Mayoral, Ben R. Davies, Pei-liang Zhao, Damien Hanlon, Elton J. G. Santos, Mikhail I. Katsnelson, Werner J. Blau, Christoph Gadermaier, and Jonathan N. Coleman, Acs Nano **10** (1), 1589 (2016).
[32] Claudia Backes, Keith R. Paton, Damien Hanlon, Shengjun Yuan, Mikhail I. Katsnelson, James Houston, Ronan J. Smith, David McCloskey, John F. Donegan, and Jonathan N. Coleman, Nanoscale **8** (7), 4311 (2016).
[33] A. C. Ferrari, J. C. Meyer, V. Scardaci, C. Casiraghi, M. Lazzeri, F. Mauri, S. Piscanec, D. Jiang, K. S. Novoselov, S. Roth, and A. K. Geim, Physical Review Letters **97** (18) (2006).
[34] S. Reich, A. C. Ferrari, R. Arenal, A. Loiseau, I. Bello, and J. Robertson, Phys Rev B **71** (20) (2005).
[35] S. De and J. N. Coleman, Acs Nano **4** (5), 2713 (2010).
[36] Graeme Cunningham, Damien Hanlon, Niall McEvoy, Georg S. Duesberg, and Jonathan N. Coleman, Nanoscale **7** (1), 198 (2015).
[37] Graeme Cunningham, Umar Khan, Claudia Backes, Damien Hanlon, David McCloskey, John F. Donegan, and Jonathan N. Coleman, J. Mater. Chem. C **1** (41), 6899 (2013).
[38] K.K. Kim, A. Hsu, X. Jia, S.M. Kim, Y. Shi, M. Dresselhaus, T. Palacios, and J. Kong, Acs Nano **6** (10), 8583 (2012).